Extreme Learning Machine Model for State-of-Charge Estimation of Lithium-Ion Battery Using Gravitational Search Algorithm

Molla S. Hossain Lipu 🔟, *Student Member, IEEE*, Mahammad A. Hannan 🔟, *Senior Member, IEEE*, Aini Hussain 🔟, *Member, IEEE*, Mohamad H. Saad, Afida Ayob, and Mohammad Nasir Uddin 🔟, *Senior Member, IEEE*

Abstract—This paper develops a state-of-charge (SOC) estimation model for a lithium-ion battery using an improved extreme learning machine (ELM) algorithm. ELM is suitable for an SOC estimation since the ELM algorithm has fast estimation speed, good generalization performance, and high accuracy. However, the performance of ELM is highly dependent on training accuracy and the number of neurons in a hidden layer. Hence, a gravitational search algorithm (GSA) is applied to improve the ELM computational intelligence by searching for the optimal value hidden layer neurons. The optimal ELM-based GSA model does not require internal battery knowledge and mathematical model for an SOC estimation. The model robustness is validated at different temperatures using different electric vehicle drive cycles. The performance of the ELM-GSA model is verified with two popular neural network methods: back-propagation neural network (BPNN) and radial basis function neural network (RBFNN). The results are evaluated using different error rates and computation costs. The results demonstrate that the ELM-based GSA model offers a higher accuracy and lower SOC error rate than those of BPNN-based GSA and RBFNN-based GSA models. Furthermore, a detailed comparative study between the proposed model and existing SOC strategies is conducted, which also demonstrates the superiority of the proposed model.

Index Terms—Electric vehicle, extreme learning machine, gravitational search algorithm, lithium-ion NMC battery, state of charge (SOC).

I. INTRODUCTION

GLOBAL emissions and climate change problems are a serious threat to human life. In order to reduce the carbon emissions, many developed countries around the world have already announced to substitute diesel- and petrol-based vehicles with electric vehicles (EVs) in near future [1]. However, the EV is still struggling to become a popular and efficient mode of transportation due to the short travel distance and limited lifecycles of energy-storage devices [2]. The performance of an EV depends on reliability, safety, driving range, and power management system, and most importantly, it is highly dependent on energy-storage functionality to predict and control critical health issues. Hence, the research on energy-storage technologies in EVs needs intensive studies to improve the performance [3]. In addition, further, development is required to increase the storage capacity, minimize the catastrophic failures, and incorporate a substantial balance to meet the operational requirements.

The lithium-ion battery has superior features such as long lifespan, high voltage and energy capacity, fast changing, and low-memory effect characteristics that outperform other energy-storage devices [4]. The prognostic model development for a lithium-ion battery with the estimation of the state-of-charge (SOC), state-of-health (SOH), and remaining useful life prediction has been researched thoroughly in recent days. Among the various components of the battery management system (BMS), SOC is a vital parameter of the lithium-ion battery, which indicates how much charge is available inside a battery cell. SOC delivers information about the driving mileage of EVs. SOC is significant to control the overcharging and overdischarging of lithium-ion cells. However, there are internal and external challenges, which cause difficulties to develop an accurate SOC estimation model. The internal challenges relate to the lithium-ion battery material, self-discharge, aging, thermal runway, and hysteresis whereas the external issues are the ambient temperature variation and charging approach. The lithium-ion battery is very sophisticated to the said challenges. Therefore, further research on SOC model development is required to extend the battery lifecycles and improve the EV performance. The mathematical expression of SOC is shown as [5]

$$\text{SOC} = \text{SOC}_0 - \frac{1}{C_n} \int i \cdot \eta dt \qquad (1)$$

where SOC_0 and SOC represent the initial value and estimated value, respectively, C_n denotes the nominal capacity, t is the duration of battery charging and discharging, and η denotes the coloumbic efficiency.

Different SOC estimation approaches have been highlighted in many articles. However, each approach has some drawbacks. The Coloumb counting is the easiest method that can estimate SOC using current integration [6]. Nevertheless, the Coloumb counting method has cumulative effect problems [7]. Open circuit voltage (OCV) holds a relationship with SOC. Nonetheless, the OCV method needs a lengthy duration to reach a balanced condition. The Kalman filter is a well-known method for SOC estimation due to its capability to reduce high fluctuation and noises in current and voltage measurements [8]. Nevertheless, the Kalman filter depends on the battery model and mathematical relationship, which may not be appropriate for highly nonlinear systems. Fuzzy logic and artificial neural network use computational intelligence to estimate SOC with noise, aging, and temperature effects [9]. Nonetheless, both methods need a large memory device and an expensive processor for implementation.

To overcome the above-mentioned problems, an optimized intelligent algorithm is proposed under the EV load profile with temperature effects. The machine-learning algorithms are useful and effective in SOC estimation since they can predict battery nonlinear dynamics without the need of any mathematical and battery model. They also have efficient computational capability that can deliver accurate results in changing conditions such as battery aging and ambient temperature. Several machine-learning algorithm based SOC estimation techniques have been explored such as radial basis function neural network (RBFNN) [10] and back-propagation neural network (BPNN) [11]. However, the network parameter selection in the said methods was performed using ineffective trial and error method, which was inefficient and wasted a lot of time and human energy. Furthermore, the algorithms suffered from low or high variance in data computation and slow computation. To address the above-mentioned challenges, this paper has proposed an extreme learning machine (ELM), which has good learning skill, high accuracy, and fast response in training execution [12]. Nonetheless, the ELM algorithm needs to find out the best value of neurons in the hidden layer to achieve high accuracy in SOC estimation. Hence, the gravitational search algorithm (GSA) is employed to improve the computational intelligence of the ELM algorithm. Du *et al.* [13] estimated SOC using the ELM method for a lithium-ion battery. Nonetheless, the hidden neurons were determined randomly, which was not reasonable for obtaining good results. Therefore, this paper has developed an improved SOC estimation model using ELM-based GSA by selecting appropriate activation function, training algorithm, and optimal number of hidden neurons to obtain high accuracy. This paper offers the following novel contributions.

1) A new ELM-based GSA model has been developed, which can evaluate SOC accurately and directly by measuring signals from the battery such as current, voltage, and temperature, hence avoiding added filter and algorithm such as the Kalman filter used in the conventional approach.
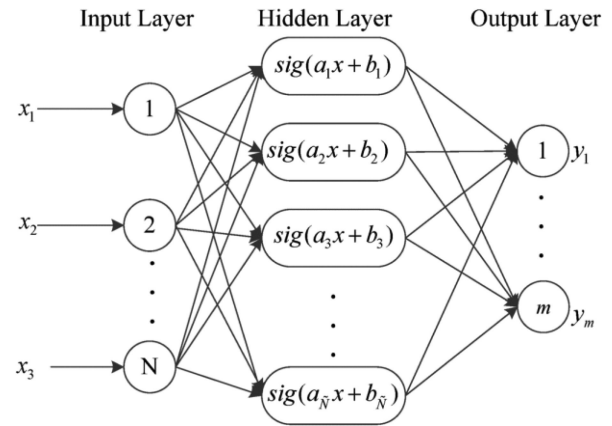

Fig. 1. Single-layer ELM model structure.

2) The input weights and the hidden layer are estimated by the self-learning ELM algorithm. The process is completely different from the electrochemical battery model, which needs practical experience and considerable time for parameter estimation.

3) The conventional GSA-based SOC estimation model uses an exhaustive trial and error approach to search for the hidden neurons. The outcomes of this traditional approach are not satisfactory due to the underfitting and overfitting problems. Therefore, the ELM algorithm is further improved by employing GSA to enhance the computational intelligence, robustness, and accuracy.

4) ELM has faster computation speed than those of other machine-learning methods, as will be revealed in the results section. Nonetheless, the standard or random value of hidden neurons causes substantial delay in estimation speed while considering the battery uncertainties including temperatures, drive cycles, and noises. The implementation of ELM with GSA has addressed the problem by determining the appropriate value of hidden layer neurons accordingly in different operating conditions, thus achieving fast acceleration in computation speed.

5) It will be shown that ELM has better generalization performance than those of other machine-learning algorithms at different conditions.

II. EXTREME LEARNING MACHINE

ELM is appropriate for predicting outcomes in complex and nonlinear systems [14]. ELM has a number of advantageous features such as better scalability, better generalization performance for regression and classification, better approximation of any target continuous function, lower computation complexity, and faster learning speed, which help to deliver better estimation results than those of other machine-learning algorithms [15], [16]. ELM is designed using three layers, one input layer, one hidden layer, and one output layer. The execution of ELM is performed by randomly assigning the input weights and hidden layers biases. The neurons in hidden layers are set adaptively. The structure of ELM is shown in Fig. 1. The steps of ELM are described as follows [17].

1) At first, the parameters are assigned randomly. The input weight vector and hidden layer bias are represented as $x_i = [x_{i1}, x_{i2}, \ldots, x_{iN}]^T$ and b_i, respectively, where i is the number of neurons in the hidden layer. The hidden neurons are assigned as $\tilde{N}$. The value of $\tilde{N}$ can be changed in order to achieve reasonable accuracy.

2) Calculate the output matrix of the hidden layer. The mathematical expression is represented by

$$\sum_{i=1}^{\tilde{N}} \beta_i f_i (x_i) = \sum_{i=1}^{\tilde{N}} \beta_i f (a_i \cdot x_j + b_j) = t_j , \ j = 1, \ldots, N \tag{2}$$

where $a_i = [a_{i1}, a_{i2}, \ldots, a_{in}]^T$ represents the weight vector that connects the input nodes and ith hidden nodes. $\beta_i = [\beta_{i1}, \beta_{i2}, \ldots, \beta_{in}]^T$ represents the output weight that connects the ith hidden layer neuron and output layer neuron. $f ()$ is the activation function that is determined before training. In this paper, the most popular sigmoid function is used for the activation function [18]

$$f (a_i \cdot x_j + b_j) = \frac{1}{1 + e^{-(a_i \cdot x_j + b_j)}}^{-1},$$
$$i = 1, \ldots, L, \ j = 1, \ldots, N \tag{3}$$

Equation (2) can be represented compactly as

$$H\beta = T \tag{4}$$

where $H(a_1, \ldots, a_{\tilde{N}}, b_1, \ldots, b_{\tilde{N}}, x_1, \ldots, x_N)$

$$H = \begin{bmatrix} f (a_1 \cdot x_1 + b_1) & \ldots & f (a_{\tilde{N}} \cdot x_1 + b_{\tilde{N}}) \\ \ldots & \ldots & \ldots \\ f (a_1 \cdot x_N + b_1) & \ldots & f (a_{\tilde{N}} \cdot x_N + b_{\tilde{N}}) \end{bmatrix}_{N \times N}$$

$$\beta = \begin{bmatrix} \beta_1^T \\ . \\ . \\ . \\ \beta_N^T \end{bmatrix}_{N \times m} \quad T = \begin{bmatrix} t_1^T \\ . \\ . \\ . \\ T_N^T \end{bmatrix}_{N \times m}.$$

H is the matrix of the output layer of the neural network.

3) The hidden layer output matrix H is determined by randomly allocated input weights and hidden layer biases. Hence, the following linear equation $H\beta = T$ is obtained:

$$\|H (a_1, \ldots, a_{\tilde{N}} b_1, \ldots, b_{\tilde{N}}) \hat{\beta} - T\| =$$
$$\min_{\beta} \|H (a_1, \ldots, a_{\tilde{N}}, b_1, \ldots, b_{\tilde{N}}) \hat{\beta} - T\|. \tag{5}$$

The least square solution is used to solve (5). The output weight β is estimated by

$$\hat{\beta} = H^+ T \tag{6}$$

where H^+ is the Moore–Penrose generalized inverse of H [19]. The optimal solution $\hat{\beta}$ features the lower training error and optimal generalization performance.

It is apparent from the above-mentioned equations, ELM needs lesser computation than those in other algorithms since it
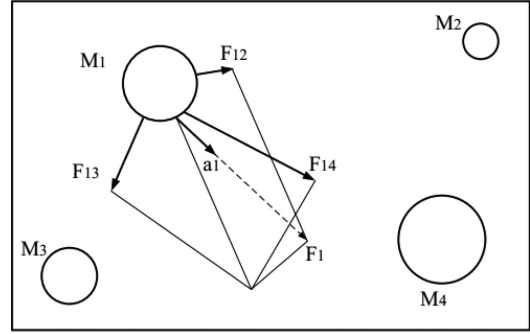

Fig. 2.   Mass effects with other masses.

uses forward pass with a series of matrix multiplications, which results in substantial development in training speed. This unique characteristic of GSA is very useful for estimating SOC with high accuracy.

III. Gravitational Search Algorithm

Rashedi *et al.* [20] invented the GSA method in 2009 to achieve an optimal solution in any complex system. They applied the concept of physics-based algorithms, such as the law of gravity and mass interactions to develop GSA. GSA is based on the law of Newtonian gravity and laws of motion. The principle of GSA states that "every particle in the universe attracts every other particle with a force that is directly proportional to their masses and inversely proportional to the square of the distance between them," as expressed in the following equation [20]:

$$F = G \frac{M_1 M_2}{R^2} \tag{7}$$

where F denotes the magnitude of the gravitational force, G represents the gravitational constant, M_1 and M_2 characterize the mass of the first and second particles, respectively, and R is the distance between the two particles.

Newton's second law states a relationship between acceleration, force, and mass of particle, which is expressed as follows:

$$a = \frac{F}{m} . \tag{8}$$

A new term named Gravitational constant $G(t)$ is introduced, which is assessed using the initial value of the gravitational constant $G(t_0)$ and the ratio of initial time t_0 and actual time t as follows:

$$G (t) = G (t_0) \times \left(\frac{t_0}{t} \right), \quad \beta < 1. \tag{9}$$

Fig. 2 shows how the influence of mass forces between the particles develop the net force and acceleration.

The positions of the N number of the agents are initialized as follows:

$$X_i = (X_i^1, \ldots, X_i^d, \ldots, X_i^n) , \quad \text{for } i = 1, 2, \ldots, N \tag{10}$$

where X_{di} is the position of ith agent in the dth dimension and n is the space dimension. The mathematical equations for the best

and worst values and the masses of each agent are presented as

$$\text{best}(t) = \text{minfit}_j(t) \tag{11}$$

$$\text{Worst}(t) = \text{maxfit}_j(t) \tag{12}$$

$$m_i(t) = \frac{\text{fit}_i(t) - \text{Worst}(t)}{\text{best}(t) - \text{Worst}(t)} \tag{13}$$

$$M_i(t) = \frac{m_i(t)}{\sum_{j=1}^{N} m_i(t)}. \tag{14}$$

The total force F for the ith agent is evaluated based on the gravitational constant G, position X, and acceleration a, and then, the velocity and position are updated

$$G(t) = G_0 \, e^{(-\alpha t/T)} \tag{15}$$

$$F_{ij}^d(t) = G(t) \frac{M_{pi} \times M_{\alpha j}}{R_{ij} + \varepsilon} \left(X_j^d(t) - X_i^d(t)\right) \tag{16}$$

$$F_i^d(t) = \sum_{j \in K\text{best}, j \neq i} \text{rand}_j \, F_{ij}^d(t) \tag{17}$$

$$a_i^d(t) = \frac{F_i^d(t)}{M_i(t)} \tag{18}$$

$$v_i^d(t+1) = \text{rand}_i \times v_i^d(t) + a_i^d(t) \tag{19}$$

$$x_i^d(t+1) = x_i^d(t) + v_i^d(t+1). \tag{20}$$

GSA is dominant in comparison to other optimization algorithms in terms of easy execution, fast learning speed, small training error, and better generalization performance [20]. In addition, GSA delivers straightforward solutions and does not have issues like inappropriate learning rate, local minima, and overfitting [21]. The flowchart of GSA is presented in Fig. 3.

IV. MODELING METHODOLOGY

First, SOC estimation for a lithium-ion battery begins with the establishment of a battery test bench followed by data collection. Beijing Dynamic Stress Test (BJDST) and US06 drive cycles are used in this paper. SOC has a high correlation with current, voltage, and temperatures; hence, these variables are selected for developing the input dataset. The consecutive drive cycles are chosen since a higher number of data are required for data training. In order to validate the model adaptability and robustness, the data are recorded in two different temperatures (25 °C and 45 °C). The data normalization is executed before the training process is started. The entire datasets of BJDST and US06 cycles are categorized into two groups: training and testing. About 70% data are employed for model training and the remaining unseen 30% data are used for data testing. The overall methodological framework of ELM-based GSA for SOC estimation is illustrated in Fig. 4. The flowchart has three phases. Phase 1 describes the data collection method. Phase 2 covers the GSA execution process. Phase 3 highlights the SOC estimation and validation process.

ELM training process is combined with GSA in order to find the appropriate number of hidden layer neurons. The lowest fitness function determines the best value of hidden layer neurons.
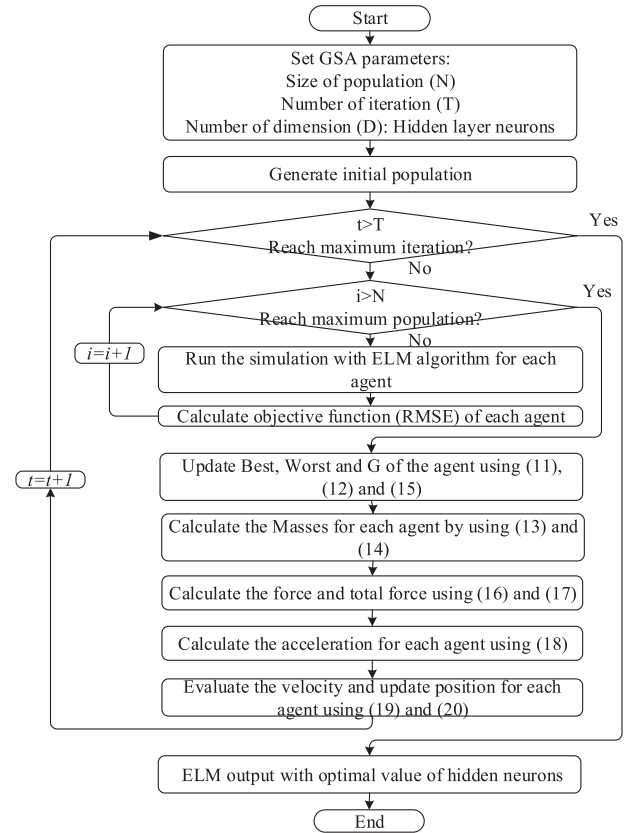

Fig. 3. Flow diagram of GSA.

The combination of ELM and GSA enhances the accurateness and efficiency of SOC, which confirms the best data fitting for the training function and delivers results with less error and less variance. Finally, SOC is assessed with testing data and ELM activation function together with an optimal number of neurons achieved from GSA. After SOC estimation, the proposed model is validated using computation cost and error rates. Finally, a comprehensive comparative investigation between the proposed ELM-GSA model and popular SOC estimation methods is performed and analyzed.

Phase I: Phase I covers the experimental arrangement, input variables selection, and data collection at different temperatures. Three significant factors including voltage, current, and temperature are chosen. The following steps are conducted in Phase I.

1) The experimental setup for SOC estimation of a lithium-ion battery is illustrated in Fig. 5. A battery test bench was established using a battery cycler (Arbin BT2000), lithium-ion battery, thermal chamber, and a host computer. The experiment was conducted using 18 650 lithium nickel manganese cobalt oxide (LiNiMnCoO$_2$ or NMC). Arbin BT2000 was employed to protect the NMC cell from being overcharged and undercharged. The thermal chamber was used to change the temperature as well as to monitor and record the temperature of the NMC cell. The SOC was examined at 25 °C and 45 °C. All the data variations were observed in the one-second interval and
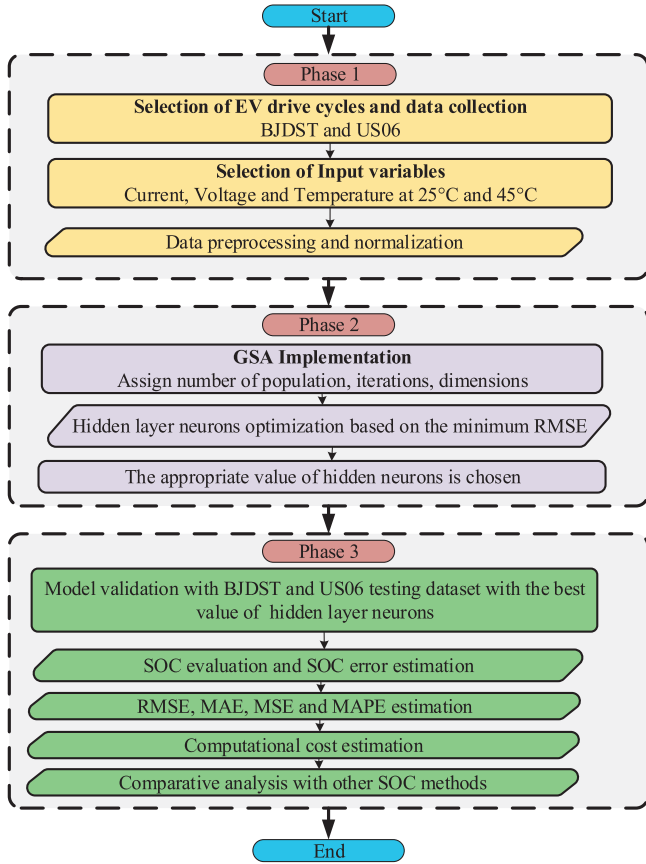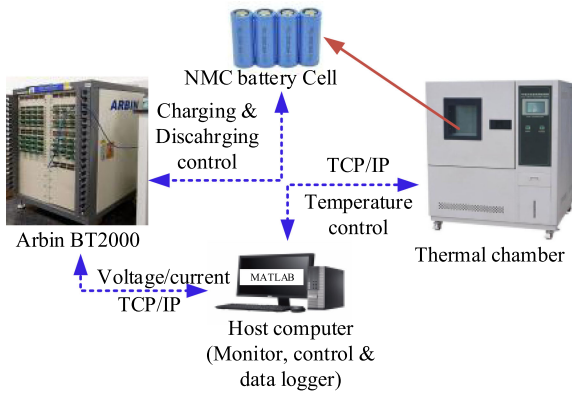
Fig. 4. Flowchart of the ELM-based GSA model.
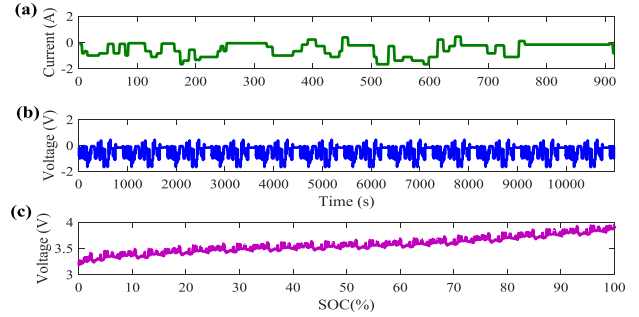

Fig. 5. Schematic diagram of battery test bench.

Fig. 6. BJDST drive cycle input dataset (a) current in one cycle, (b) voltage, and (c) voltage against SOC.
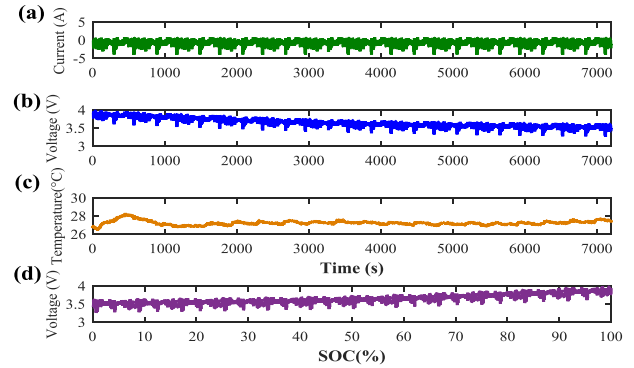

Fig. 7. US06 rive cycle input dataset (a) current, (b) voltage, (c) temperature, and (d) voltage against SOC.

controlled by the host computer. The verification of the proposed model in a real-time EV application was tested using BJDST [22] and US06 [23] drive cycles. The driving time to complete one BJDST cycle and one US06 cycle is 916 s and 600 s, respectively [22]. Battery discharge and data extraction were conducted using 12 consecutive BJDST and US06 cycles.

2) BJDST and US06 cycles are loaded to extract features at two different temperatures (25 °C and 45 °C).

3) Data normalization is important in ELM training since it accelerates the training speed and helps the algorithm

to become more efficient and robust. The normalization data process is expressed in (21) where the length is set to $[-1,1]$

$$x = \frac{2\left(x - x_{\min}\right)}{x_{\max} - x_{\min}} \tag{21}$$

where the maximum and minimum value of the input variable x of the ELM model is denoted by $x_{\max}$ and $x_{\min}$. The training and testing datasets are scaled using the same normalization range. The input dataset of BJDST and US06 drive cycles are shown in Figs. 6 and 7, respectively.

Phase II: GSA is utilized to determine the optimal number of hidden layer neurons. The following steps are used in phase II.

1) First, the implementation of the GSA algorithm starts with the setting of parameters. In this paper, the population size (agent) and iteration number are assigned as 50 and 100, respectively. The paper also defines the limit of hidden layer neurons. The boundary is between "0" and "500."

2) The agent position of hidden layer neurons is created in a random order that is placed within the boundary range.

3) The ELM training algorithm and activation function are executed to train the data of hidden layer neurons.

4) The fitness function of each agent is evaluated. In this paper, the root mean square error (RMSE) is chosen as a fitness function due to high sample dataset and random distribution of error estimation [24].

5) The gravitational constant G and best, worst position of the agent are updated using (15)–(17).
6) Calculate the velocity and acceleration of agent using (19) and (18).
7) Update agent position using (20).
8) The training algorithm and activation function are recalled to re-evaluate the fitness function of each agent.
9) The best agent location and velocity are assessed through all the iterations based on the lowest value of fitness function. The minimum value of fitness function corresponds to the best value of hidden layer neurons.

Phase III: Phase III is called the final stage where SOC is estimated with the testing data and the optimal value of neurons achieved from GSA. The accuracy of the ELM-based GSA model is examined by various error terms. The summary of this phase is explained as follows.

1) The ELM algorithm takes the optimal value of hidden neurons and initiates training process.
2) The testing data are used to monitor SOC under 25 °C and 45 °C temperatures. SOC is estimated in both BJDST and US06 drive cycles. The estimated SOC is checked with the reference value achieved from the Coloumb counting method. In this paper, a correct sensor was calibrated carefully to avoid cumulative error. Additionally, SOC error is observed, which is calculated by the difference between the estimated SOC and reference.
3) The effectiveness of the proposed model is evaluated using various types of error rates. The error rates include RMSE, mean square error (MSE), mean absolute error (MAE), and mean absolute percentage error (MAPE). The equations of these error rates are presented as follows:

$$\text{RMSE} = \sqrt{\frac{1}{N}\sum_{i=1}^{N}\left(I_{\text{es}} - I_a\right)^2} \qquad (22)$$

$$\text{MSE} = \frac{1}{N}\sum_{i=1}^{N}\left(I_{\text{es}} - I_a\right)^2 \qquad (23)$$

$$\text{MAE} = \frac{1}{N}\sum_{i=1}^{N}\left(I_{\text{es}} - I_a\right) \qquad (24)$$

$$\text{MAPE} = \frac{1}{N}\sum_{i=1}^{N}\left|\frac{I_a - I_{\text{es}}}{I_a}\right| \qquad (25)$$

where I_{es} and I_a denote the estimated value, and actual value, respectively, and N denotes the number of observations.

V. RESULTS AND DISCUSSIONS

A. Fitness Function and Optimal Parameter

The fitness function of GSA is assessed by generating optimization response curves for BJDST and US06 cycles with 50 population size and 100 iterations, as illustrated in Figs. 8 and 9, respectively. The optimization response curves are observed at 25 °C and 45 °C temperatures. The specific iteration number
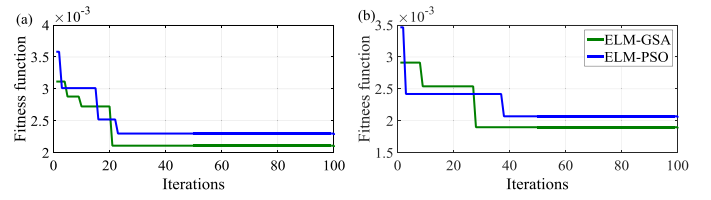

Fig. 8.   Optimization response curves of BJDST cycle (a) 25 °C and (b) 45 °C.
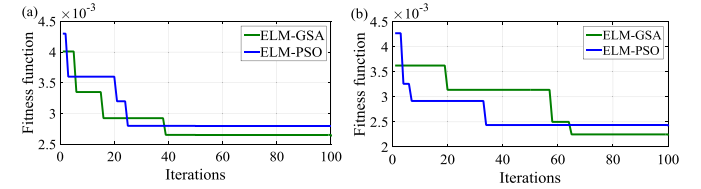

Fig. 9.   Optimization response curves of US06 cycle (a) 25 °C and (b) 45°C.
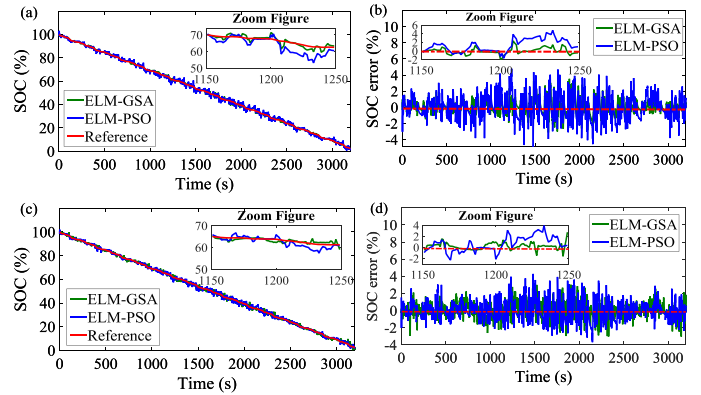

Fig. 10.   SOC and SOC error comparison between ELM-GSA and ELM-PSO; (a), (b) at 25 °C, (c), (d) at 45 °C in the BJDST cycle.

that has the lowest fitness function delivers the best value of hidden neurons. In the BJDST cycle, the lowest value of the fitness function is recorded after 20 and 27 iterations at 25 °C and 45 °C, respectively. The values of the fitness functions corresponding to the said iterations are 2.3×10^{-3} and 1.9×10^{-3}, respectively. Accordingly, the hidden neurons are estimated to be 220 and 328. In the US06 cycle, 38 and 67 iterations provide the minimum value of the fitness function amounting to 2.7×10^{-3} and 2.2×10^{-3} at 25 °C and 45 °C, respectively. The hidden neurons associated with the stated iteration are computed to be 158 and 147. The effectiveness of GSA is compared with the PSO algorithm using the same iteration and population size, in order to have a fair comparison. The results show that GSA performs better than PSO in obtaining the lowest fitness function, which ensures the high accuracy in SOC estimation. It is also evident that the fitness function declines as the temperature rises. The electrolyte activity increases with the rise in temperature. Hence, the capacity of the battery rises as the temperate accelerates.

B. SOC Evaluation Using ELM-GSA and ELM-PSO Model

The ELM-based GSA model examines SOC in BJDST and US06 cycles, as shown in Figs. 10 and 11, respectively. The SOC estimation results and SOC error rates are compared with the
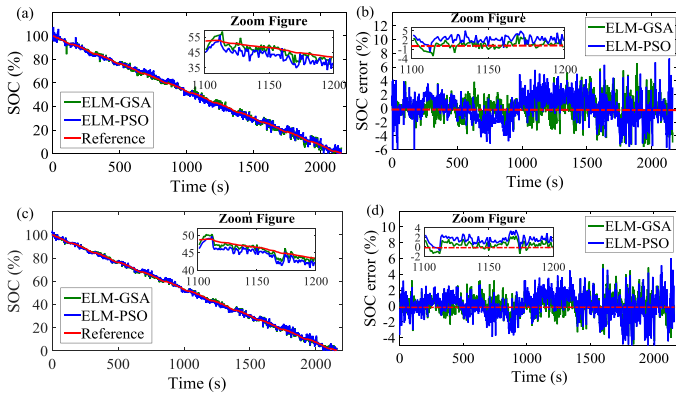
Fig. 11. SOC and SOC error comparison between ELM-GSA and ELM-PSO; (a), (b) at 25°C, (c), (d) at 45 °C in the US06 cycle.

TABLE I
PERFORMANCE ASSESSMENT IN THE BJDST CYCLE

Model	BPNN-GSA		RBFNN-GSA		ELM-GSA	
Temperature	25°C	45°C	25°C	45°C	25°C	45°C
RMSE (%)	0.95	0.87	1.12	0.97	0.76	0.68
MSE (%)	0.0087	0.0072	0.011	0.0092	0.0059	0.0052
MAE (%)	0.72	0.64	0.85	0.71	0.55	0.48
MAPE (%)	3.98	3.75	4.15	3.82	3.84	3.24
SOC Error (%)	-5.2~5.1	-4.8~4.6	-6.6~6.8	-5.3~4.9	-3.1~3.6	-2.9~3

TABLE II
PERFORMANCE ASSESSMENT IN THE US06 CYCLE

Model	BPNN-GSA		RBFNN-GSA		ELM-GSA	
Temperature	25°C	45°C	25°C	45°C	25°C	45°C
RMSE (%)	1.68	1.38	2.2	1.88	1.56	1.2
MSE (%)	0.032	0.018	0.089	0.064	0.024	0.014
MAE (%)	1.87	1.12	2.23	1.35	1.67	0.91
MAPE (%)	16.71	9.28	18.8	12.7	14.32	7.5
SOC Error (%)	-6.2~8.7	-5.1~5.7	-8.7~9.2	-6.3~6.8	-5.6~6.5	-4.8~5.3

reference. The ampere-hour method with a calibrated current sensor is chosen as a reference. Before loading EV drive cycles, NMC was fully charged and the initial SOC was set to 100%. It is seen from the figures that the estimated SOC value is almost placed to the same line of the reference value throughout the drive cycles, which demonstrate that the proposed model has high robustness and low estimation error. It is also important to monitor SOC error that signifies how much estimated SOC deviates from the reference value. The error lies at between −3.1% and 3.6% and −5.6% and 6.5% in BJDST and US06 cycles, respectively, at 25 °C. Nevertheless, in the ELM-based PSO model, the SOC error is restricted to [−5.2 ∼4.7%] in BJDST and [−7.5% ∼7%] in US06. The estimation error in US06 is higher than that of BJDST due to the high randomness and fluctuation of load current. It is also observed from the figures that the SOC error declines with the rise in temperature. The error bounds are from −2.9% to 3% in BJDST whereas in the US06 cycle, the error bounds are from −4.8% to 5.3% at 45 °C in the ELM-based GSA model. Nonetheless, the ELM-based PSO model examines SOC with a high error rate with a range of [−3.7% ∼4.3%] in BJDST and [−5.5% ∼6%] in US06. The results demonstrate that the proposed ELM-based GSA model provides more accurate results than that of the ELM-based PSO model. In addition, the ELM-based GSA model is robust and efficient in SOC estimation under different EV drive cycles and temperature conditions.

C. SOC Performance Comparison

The comparative study of SOC estimation using ELM-GSA, BPNN-GSA, and the RBFNN-GSA models for BJDST and DST cycle is depicted in Tables I and II, respectively. SOC estimation by ELM-GSA is compared with BPNN and RBFNN, as presented in Table I in BJDST and US06 cycles, respectively. In order to perform a fair comparison, BPNN and RBFNN methods use similar input dataset for training and testing. Furthermore, the hidden neurons of BPNN and RBFNN are tuned based on GSA with the same number of iterations and population sizes. In the BJDST cycle, ELM-based GSA achieves RMSE of 0.76% whereas BPNN-GSA and RBFNN-GSA models obtain RMSE of 0.95% and 1.12%, respectively, at 25 °C. However, the lower error rates and SOC error are observed as temperature increases from 25 °C to 45 °C. The proposed model computes RMSE to be 0.68% at 45 °C, which is reduced by 21.8% and 29.8% from the BPNN-GSA and RBFNN-GSA model, respectively. An improvement is also noticed in MSE, MAE, and MAPE in the ELM-GSA model under different drive cycles. The MSE of the proposed model is estimated to be 0.0059% that is dropped by 32.2% and 46.4% from BPNN-GSA and RBFNN-GSA models, respectively, at 25 °C. Similarly, about 23.6% and 35.3% reductions are noted in BPNN-GSA and RBFNN-GSA models, respectively, at 25 °C compared with the ELM-GSA model while assessing MAE. In addition, MAPE in BPNN-GSA and RBFNN-GSA models become higher and raised by 3.6% and 8.1%, in comparison to the ELM-GSA model at 25 °C. The estimation results of the proposed model are further evaluated using the US06 cycle. RMSE in BPNN-GSA and RBFNN-GSA models is measured to be 1.68% and 2.2%, respectively, which is a 7.7% and 41% rise from the ELM-GSA model. Moreover, there is a drop of 10.7% and 25.1% in MAE in the proposed model in comparison with the other two models at 25 °C. Furthermore, ELM-GSA obtains a 14.3% and 23.8% reduction in MAPE in comparison with the other two models at 25 °C.

D. Computational Cost

In order to implement the ELM-based GSA algorithm through the on-board BMS with low data processing, limited storage, and power requirement, the computational cost of SOC estimation needs to be investigated. The algorithm is executed on Core i5 2.3 GHz processor with 12 GB RAM and repeated for ten times to achieve the average computing time. The computational cost of SOC estimation comprises both training and testing times [25]. The results displayed in Table III demonstrate that the ELM-based GSA has a fast response to data training whereas BPNN and RBFNN models need a long time in training for weight and bias upgradation. Since the average execution time is less than 1 s, the proposed ELM-based GSA model for SOC estimation is verified to be appropriate for on-board BMS implementation.

TABLE III
COMPUTATIONAL COST IN BJDST AND US06 DRIVE CYCLES

Method	EV Cycle	Temperature	Computational cost (s)
BPNN-GSA	BJDST	25°C	8.3573
		45°C	8.3915
	US06	25°C	5.7225
		45°C	5.7462
RBFNN-GSA	BJDST	25°C	13.9742
		45°C	13.9941
	US06	25°C	6.2272
		45°C	6.2494
ELM-GSA	BJDST	25°C	0.5156
		45°C	0.5938
	US06	25°C	0.2188
		45°C	0.2656

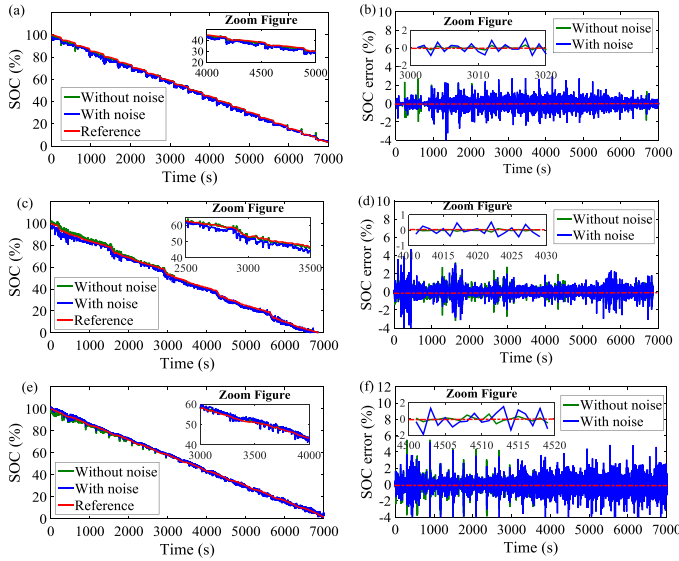Fig. 13. SOC robustness comparison under different drive cycles.

Fig. 12. SOC estimation and SOC error with and without noise under (a), (b) DST cycle, (c), (d) FUDS cycle, and (e), (f) US06 cycle.

E. Robustness Against Different Testing Dataset

The robustness of the ELM-based GSA model is validated with different testing drive cycles. The model is trained by a BJDST cycle and then tested by Dynamic Stress Test (DST) [26], Federal Urban Driving Schedule (FUDS) [27], and the US06 cycle at 25 °C, as shown in Fig. 12.

Moreover, low sensor precision and electromagnetic interference might result in inaccurate battery data measurements. Therefore, it is important to evaluate the robustness against the measurement noise. The common white Gaussian noise with zero mean is added to the measured values to evaluate the proposed model suitability in the real world. A standard random noise of 0.1 A and 0.01 V is added to current and voltage measurements, respectively. Furthermore, a 0.1 A and 0.01 V positive bias noise is injected to the current and voltage measurements. Due to the high nonlinearity of current signal in the drive cycles, high error spike is noticed after certain intervals. Hence, a moving average filter is used to reduce the maximum absolute error and smooth out the estimated SOC. It is noticed in Fig. 12 that the SOC error bounds in DST, FUDS, and US06 are [−2.3∼2.7], [−3.1∼3.2] and [−4.8∼5.5], respectively. Moreover, the estimated SOC by three drive cycles are also almost

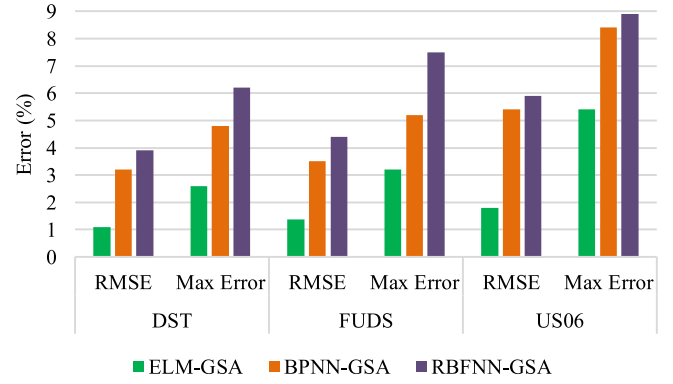aligned with the actual SOC. However, a few oscillations are observed in SOC estimation with the noise effect inclusion. Likewise, there is a small rise in the SOC error when the random noise and bias noise are considered. Although there is a bit increase in the SOC error rate, the performance inconsistency is within the satisfactory limit. To sum up, the proposed model has proven to be a generalized machine-learning algorithm, which has strong robustness not only under different drive cycles but also against the measurement noise.

The robustness of the ELM-GSA model is further checked with the BPNN-GSA and RBFNN-GSA models under different testing datasets. Fig. 13 shows the comparative analysis where performance is assessed in terms of RMSE and maximum SOC error without noise effect at 25 °C.

It is observed from Fig. 13 that there is a significant performance improvement in the ELM-GSA model, having RMSE of 1.1%, 1.4%, and 1.8% in DST, FUDS and US06 cycles, respectively. However, the BPNN-GSA and RBFNN-GSA models achieve a fairly high RMSE, amounting to 3.2%, 3.5%, 5.4% and 3.9%, 4.4%, 5.9% in DST, FUDS, and US06 cycle, respectively, which is approximately 2–3 times as much as the ELM-GSA model. The proposed ELM-GSA model also performs satisfactorily in achieving the maximum SOC error, which is limited between 2.6% and 5.4% under different drive cycles. Nevertheless, the maximum error rate is increased substantially and is bounded from 4.8% to 8.4% and from 6.2% to 8.9% in the BPNN-GSA and RBFNN-GSA models, respectively. On a whole, the ELM-GSA model has better results on accuracy and robustness than those of the BPNN-GSA and RBFNN-GSA models.

VI. COMPARATIVE VALIDATION WITH OTHER METHODS

The accuracy and robustness of the ELM-GSA method is further validated by investigating the SOC error terms between the developed model and other prominent SOC methods. Seven recent and prominent studies including backtracking search algorithm (BSA), Kalman filter, fuzzy logic, neural network, deep learning, and support vector machine are considered for comparative evaluation, as presented in Table IV. It is evident from Table IV that the ELM-based GSA model has a better performance and robustness than those of other existing approaches under different operating conditions. For instance, the RMSE

TABLE IV
COMPARATIVE PERFORMANCE ASSESSMENT OF SOC ESTIMATION

No.	Method	Ref.	Test Battery	Validation Profile	Temperature	Error Rate
1.	OCV	[28]	18650 cylindrical type 1.1 Ah lithium-ion cells (LiFePO$_4$)	Federal Urban Driving Schedule (FUDS)	0 °C to 50 °C at an interval of 10 °C.	RMSE < 5%
2.	Electrochemical Model (ECM)	[29]	3 Ah LiFePO$_4$ cell	Urban Dynamometer Driving Schedule (UDDS)	25°C	SOC error < 5% in different RC networks
3.	Kalman Filter (KF)	[30]	20 AH A123 cylindrical 26650 Li-ion batteries	US06 drive cycle	25°C (ambient temperature)	SOC error <4%
4.	H∞ filter	[31]	1.2 Ah lithium-ion battery	Pulse charging and discharging	Room temperature	RMSE under 2.5%
5.	BPNN based BSA	[32]	2 Ah 18650 LiNiMnCoO$_2$/NMC	(i) FUDS (ii) Dynamic Stress Test (DST)	0°C, 25°C and 45°C	RMSE 0.57%~1.74% in FUDS RMSE 0.48% ~1.47% in DST
6.	Deep Learning	[33]	2.9 Ah Panasonic LiNiCoAlO$_2$/ NCA	Dynamic drive cycles, ±18 A,	0°C, 10°C and 25°C	RMSE 1.11% ~2.44% MAE 0.77%~2.08%
7.	ANFIS	[34]	40 Ah, 36 Lithium-Ion cells	Charging and discharging currents (i) 57 A, (ii) 68 A	Temperature range from -30 °C to 55 °C	MSE 3.4% in 57 A MSE 5.6% in 68A
8.	ELM based GSA (proposed in this study)	-	2 Ah 18650 LiNiMnCoO$_2$/NMC	(i) DST (ii) FUD (ii) US06	25°C	RMSE of 1.1% in DST RMSE 1.4% in FUDS RMSE 1.8% in US06

using BPNN with the BSA model is estimated under 2% in the FUDS cycle. Nonetheless, the ELM-based GSA model delivers more accurate SOC estimation results, with RMSE being less than 1.5% in FUDS cycles. Similarly, the ELM-based GSA model is dominant in comparison to deep-learning method, fuzzy logic, Kalman filter, H∞ filter, and SVM methods.

VII. CONCLUSION

The overall contribution is the development of an intelligent SOC estimation model using ELM with GSA that obtains improved performance in improving the robustness, increasing the accuracy, and accelerating the estimation speed under different EV drive cycles, temperatures, and measurement noises. The performance of GSA is compared with the PSO algorithm, where GSA outperforms PSO in reaching the lowest fitness function. The robustness of the developed model is verified using two EV drive profiles at different temperatures. The SOC accuracy is improved significantly with RMSE below 1% in the BJDST cycle and 1.6% in the US06 cycle. Moreover, the computation speed is achieved within one second. In addition, the proposed model shows superior performance when it is validated with different drive cycles and noise effects. RMSE and maximum SOC error are estimated below 2% and 5.5%, respectively. A detailed comparative investigation in Table IV also indicates that the developed model is dominant in comparison to other approaches in obtaining high adaptability, efficiency, precision, robustness, and estimation cost. Our future research will assess SOH for the lithium-ion battery with aging effects. Besides, the future work will compare the ELM model based SOC estimation performance with other machine-learning approaches. Moreover, the comparative performance evaluation of GSA with other optimization techniques will also be studied.

REFERENCES

[1] M. A. Hannan, M. S. H. Lipu, A. Hussain, and A. Mohamed, "A review of lithium-ion battery state of charge estimation and management system in electric vehicle applications: Challenges and recommendations," *Renew. Sustain. Energy Rev.*, vol. 78, pp. 834–854, 2017.

[2] M. S. H. Lipu, A. Hussain, M. H. M. Saad, A. Ayob, and M. A. Hannan, "Improved recurrent NARX neural network model for state of charge estimation of lithium-ion battery using pso algorithm," in *Proc. IEEE Symp. Comput. Appl. Ind. Electron.*, 2018, pp. 354–359.

[3] M. A. Hannan, M. M. Hoque, A. Mohamed, and A. Ayob, "Review of energy storage systems for electric vehicle applications: Issues and challenges," *Renew. Sustain. Energy Rev.*, vol. 69, pp. 771–789, 2017.

[4] D. Ansean, M. Gonzalez, V. M. Garcia, J. C. Viera, J. C. Anton, and C. Blanco, "Evaluation of LiFePO$_4$ batteries for electric vehicle applications," *IEEE Trans. Ind. Appl.*, vol. 51, no. 2, pp. 1855–1863, Mar./Apr. 2015.

[5] M. S. H. Lipu, M. A. Hannan, A. Hussain, M. H. M. Saad, A. Ayob, and F. Blaabjerg, "State of charge estimation for lithium-ion battery using recurrent NARX neural network model based lighting search algorithm," *IEEE Access*, vol. 6, pp. 28150–28161, 2018.

[6] K. S. Ng, C. S. Moo, Y. P. Chen, and Y. C. Hsieh, "Enhanced Coloumb counting method for estimating state-of-charge and state-of-health of lithium-ion batteries," *Appl. Energy*, vol. 86, no. 9, pp. 1506–1511, 2009.

[7] M. Coleman, C. K. Lee, C. Zhu, and W. G. Hurley, "State-of-charge determination from EMF voltage estimation: Using impedance, terminal voltage, and current for lead-acid and lithium-ion batteries," *IEEE Trans. Ind. Electron.*, vol. 54, no. 5, pp. 2550–2557, Oct. 2007.

[8] Z. Chen, Y. Fu, and C. C. Mi, "State of charge estimation of lithium-ion batteries in electric drive vehicles using extended Kalman filtering," *IEEE Trans. Veh. Technol.*, vol. 62, no. 3, pp. 1020–1030, Mar. 2013.

[9] I.-H. Li, W.-Y. Wang, S.-F. Su, and Y.-S. Lee, "A merged fuzzy neural network and its applications in battery state-of-charge estimation," *IEEE Trans. Energy Convers.*, vol. 22, no. 3, pp. 697–708, Sep. 2007.

[10] L. Kang, X. Zhao, and J. Ma, "A new neural network model for the state-of-charge estimation in the battery degradation process," *Appl. Energy*, vol. 121, pp. 20–27, 2014.

[11] S. Tong, J. H. Lacap, and J. W. Park, "Battery state of charge estimation using a load-classifying neural network," *J. Energy Storage*, vol. 7, pp. 236–243, Aug. 2016.

[12] G. Bin Huang, Q. Y. Zhu, and C. K. Siew, "Extreme learning machine: Theory and applications," *Neurocomputing*, vol. 70, no. 1–3, pp. 489–501, 2006.

[13] J. Du, Z. Liu, and Y. Wang, "State of charge estimation for Li-ion battery based on model from extreme learning machine," *Control Eng. Pract.*, vol. 26, no. 1, pp. 11–19, 2014.

[14] M. S. H. Lipu, M. A. Hannan, A. Hussain, M. H. M. Saad, A. Ayob, and M. N. Uddin, "Extreme learning machine for SOC estimation of lithium-ion battery using gravitational search algorithm," in *Proc. IEEE Ind. Appl. Soc. Annu. Meeting*, 2018, pp. 1–8.

[15] G.-B. Huang, H. Zhou, X. Ding, and R. Zhang, "Extreme learning machine for regression and multiclass classification," *IEEE Trans. Syst. Man, Cybern. B*, vol. 42, no. 2, pp. 513–529, Apr. 2012.

[16] A. M. A. Sattar, Ö. F. Ertuğrul, B. Gharabaghi, E. A. McBean, and J. Cao, "Extreme learning machine model for water network management," *Neural Comput. Appl.*, vol. 31, no. 1, pp. 157–169, Jan. 2019.

[17] G.-B. Huang, D. H. Wang, and Y. Lan, "Extreme learning machines: A survey," *Int. J. Mach. Learn. Cybern.*, vol. 2, no. 2, pp. 107–122, Jun. 2011.

[18] G. Bin Guang-Bin Huang, "Learning capability and storage capacity of two-hidden-layer feedforward networks," *IEEE Trans. Neural Netw.*, vol. 14, no. 2, pp. 274–281, Mar. 2003.

[19] D. (Denis) Serre, *Matrices: Theory and Applications*. New York, NY, USA: Springer, 2010.

[20] E. Rashedi, H. Nezamabadi-pour, and S. Saryazdi, "GSA: A gravitational search algorithm," *Inf. Sci.*, vol. 179, no. 13, pp. 2232–2248, Jun. 2009.

[21] E. Rashedi, E. Rashedi, and H. Nezamabadi-pour, "A comprehensive survey on gravitational search algorithm," *Swarm Evol. Comput.*, vol. 41, pp. 141–158, Aug. 2018.

[22] M. S. Hossain Lipu, M. A. Hannan, A. Hussain, and M. H. M. Saad, "Optimal BP neural network algorithm for state of charge estimation of lithium-ion battery using PSO with PCA feature selection," *J. Renewable Sustain. Energy*, vol. 9, no. 6, Nov. 2017, Art. no. 064102.

[23] F. Zheng, Y. Xing, J. Jiang, B. Sun, J. Kim, and M. Pecht, "Influence of different open circuit voltage tests on state of charge online estimation for lithium-ion batteries," *Appl. Energy*, vol. 183, pp. 513–525, 2016.

[24] T. Chai and R. R. Draxler, "Root mean square error (RMSE) or mean absolute error (MAE)? – Arguments against avoiding RMSE in the literature," *Geosci. Model Dev.*, vol. 7, no. 3, pp. 1247–1250, Jun. 2014.

[25] H. Chaoui and C. C. Ibe-Ekeocha, "State of charge and state of health estimation for lithium batteries using recurrent neural networks," *IEEE Trans. Veh. Technol.*, vol. 66, no. 10, pp. 8773–8783, Oct. 2017.

[26] R. Xiong, F. Sun, X. Gong, and C. Gao, "A data-driven based adaptive state of charge estimator of lithium-ion polymer battery used in electric vehicles," *Appl. Energy*, vol. 113, pp. 1421–1433, Jan. 2014.

[27] W. He, N. Williard, C. Chen, and M. Pecht, "State of charge estimation for Li-ion batteries using neural network modeling and unscented Kalman filter-based error cancellation," *Int. J. Elect. Power Energy Syst.*, vol. 62, pp. 783–791, 2014.

[28] Y. Xing, W. He, M. Pecht, and K. L. Tsui, "State of charge estimation of lithium-ion batteries using the open-circuit voltage at various ambient temperatures," *Appl. Energy*, vol. 113, pp. 106–115, Jan. 2014.

[29] H. He, R. Xiong, and H. Guo, "Online estimation of model parameters and state-of-charge of LiFePO$_4$ batteries in electric vehicles," *Appl. Energy*, vol. 89, no. 1, pp. 413–420, 2012.

[30] M. Mastali, J. Vazquez-Arenas, R. Fraser, M. Fowler, S. Afshar, and M. Stevens, "Battery state of the charge estimation using Kalman filtering," *J. Power Sources*, vol. 239, pp. 294–307, 2013.

[31] M. Charkhgard and M. H. Zarif, "Design of adaptive H ∞ filter for implementing on state-of-charge estimation based on battery state-of-charge-varying modelling," *IET Power Electron.*, vol. 8, no. 10, pp. 1825–1833, 2015.

[32] M. A. Hannan, M. S. H. Lipu, A. Hussain, M. H. Saad, and A. Ayob, "Neural network approach for estimating state of charge of lithium-ion battery using backtracking search algorithm," *IEEE Access*, vol. 6, pp. 10069–10079, 2018.

[33] E. Chemali, P. Kollmeyer, M. Preindl, R. Ahmed, and A. Emadi, "Long short-term memory-networks for accurate state of charge estimation of li-ion batteries," *IEEE Trans. Ind. Electron.*, vol. 65, no. 8, pp. 6730–6739, Aug. 2017.

[34] M. A. Awadallah and B. Venkatesh, "Accuracy improvement of SOC estimation in lithium-ion batteries," *J. Energy Storage*, vol. 6, pp. 95–104, 2016.

Mahammad A. Hannan (M'10–SM'17) received the B.Sc. degree in electrical and electronic engineering from the Chittagong University of Engineering and Technology, Chittagong, Bangladesh, in 1990, the M.Sc. and Ph.D. degrees in electrical, electronic, and systems engineering from the Universiti Kebangsaan Malaysia, Bangi, Malaysia, in 2003 and 2007, respectively.

He is currently a Professor of intelligent systems with the Department of Electrical Power Engineering, College of Engineering, Universiti Tenaga Nasional, Selangor, Malaysia. He has authored or coauthored more than 300 papers in the reputed journals and proceedings and organizing chair of many conferences (International Conference on Energy & Environment 2019, International Conference on Power Engineering and Automation Engineering 2019, International Conference on Power System and Automation Engineering 2019). His research interests include intelligent controllers, power electronics, hybrid vehicles, energy-storage systems, image and signal processing, and artificial intelligence.

Dr. Hannan is an Associate Editor of IEEE Access. He is the recipient of a number of gold awards for his innovative research in International Invention, Innovation & Technology Exhibition (ITEX), Malaysia Technology Expo (MTE), International Innovation Festival (INNOFEST), Seoul International Invention Fair (SIIF), Invention and Innovation Competition of Higher Education Institutions (PERINTIS) etc.

Aini Hussain (M'98) received the B.Sc. degree in electrical engineering from Louisiana State University, Baton Rouge, LA, USA, the M Sc. degree from the University of Manchester Institute of Science and Technology, Manchester, U.K., and the Ph.D. from Universiti Kebangsaan Malaysia, Bangi, Malaysia.

She is currently a Professor with the Centre for Integrated Systems Engineering and Advanced Technologies, Faculty of Engineering and Built Environment, Universiti Kebangsaan Malaysia. Her research interests include decision support systems, machine learning, pattern precognition, and signal and image processing.

Mohamad H. Saad received the B. Sc. degree in mechanical and materials engineering and the Ph.D. degree from Universiti Kebangsaan Malaysia, Bangi, Malaysia, in 1999 and 2017, respectively.

He is currently a Senior Lecturer with the Department of Mechanical and Materials Engineering, Faculty of Engineering and Built Environment, Universiti Kebangsaan Malaysia. His research interests include artificial intelligence, intelligent systems, and complex event processing.

Afida Ayob received the B.Sc. degree in electrical and electronic engineering from the University of Manchester, Manchester, U.K., in 2000 and the Ph.D. degree from Newcastle University, Newcastle upon Tyne, U.K., in 2012.

She is currently a Senior Lecturer with the Centre for Integrated Systems Engineering and Advanced Technologies, Faculty of Engineering and Built Environment, Universiti Kebangsaan Malaysia, Bangi, Malaysia. Her research interests include power electronic, energy storage, and artificial intelligence.

Molla S. Hossain Lipu received the B.S. degree in electrical and electronic engineering from the Islamic University of Technology, Gazipur, Bangladesh, in 2008 and the M.S. degree in energy from the Asian Institute of Technology, Bangkok, Thailand, in 2013. He is currently working toward the Ph.D. degree in the Centre for Integrated Systems Engineering and Advanced Technologies, FKAB, Universiti Kebangsaan Malaysia, Bangi, Malaysia.

He is currently an Assistant Professor of electrical and electronic engineering with the University of Asia Pacific, Dhaka, Bangladesh. His research interests include energy-storage systems, artificial intelligence, model optimization, and hybrid renewable energy system.

Mohammad Nasir Uddin (S'99–M'00–SM'04) received the B.Sc. and M.Sc. degrees in electrical and electronic engineering from the Bangladesh University of Engineering and Technology, Dhaka, Bangladesh, in 1993 and 1996, respectively, and the Ph.D. degree in electrical engineering from the Memorial University of Newfoundland, St. John's, NF, Canada, in 2000.

He is currently a Professor with the Department of Electrical Engineering, Lakehead University, Thunder Bay, ON, Canada, where he is engaged in teaching and research. His research interests include power electronics, electric motor drives, and applications of neural networks.